RESEARCH ARTICLE

Implementation of an Active Vibration Control System on a Cogeneration Plant

EMANUELE VOLTOLINI [1], DANIEL PINARDI [1], ANDREA TOSCANI [1], MARCO BINELLI [1], ANGELO FARINA [1], JESSICA FERRARI[1], ANDREA ZENARO[2], STEFANO MAGLIA[2], AND ENRICO CALZAVACCA[2]

[1]Department of Engineering and Architecture, University of Parma, 43124 Parma, Italy
[2]AB Holding S.p.a., 25034 Orzinuovi, Italy

Corresponding author: Andrea Toscani (andrea.toscani@unipr.it)

ABSTRACT Active noise control (ANC) aims to reduce a noise source at a listening point by destructive interference with a reverse phase noise emitted by one or more control devices. ANC systems cover a wide range of applications, such as industrial plants, vehicle cabins, headphones. Usually, in these applications the control devices are loudspeakers, and the error signals come from microphones. In outdoor applications, this solution comes with some limitations, such as the ageing of the loudspeakers due to humidity, temperature, rain and dust, and the presence of wired connections between the error sensors and the control system. This paper presents a noise reduction solution for a cogeneration plant, consisting of an Active Vibration Control (AVC) system applied to the cogenerator enclosure. To overcome the above limitations, electrodynamic shakers are used as controllers and an accelerometer as error signal. The control algorithm is a single reference, Single Input, Multiple Output (SIMO) Filtered-X Normalized Least Mean Square (FxNLMS), implemented in a Virtual Studio Technology (VST) plugin. VST plugins work in real-time in Digital Audio Workstation (DAW) software installed on personal computers, therefore without the need for low-level implementation on dedicated electronic boards, thus reducing the development time and the cost of the equipment. First, the effectiveness of the solution is demonstrated in a laboratory experiment. Subsequently, the results obtained on the cogenerator are presented, which show remarkable performance, with a noise reduction up to -17.5 dB on the main disturbing frequencies.

INDEX TERMS Active noise control, active vibration control, cogeneration plant, electrodynamic shaker, filtered-X normalized LMS, primary path, secondary path.

I. INTRODUCTION

With the rapid growth of transportation and industrial activities, noise pollution has become a severe problem affecting the quality of human life [1], [2]. Traditional methods employ Passive Noise Control (PNC) such as sealing and shielding [3], [4]. Although these techniques are widely used, they involve excessive costs, bulky volume, and a decrease in effectiveness at lower frequencies. A valid alternative is represented by Active Noise Control (ANC)

techniques [5], which involve the use of electromechanical or electroacoustic devices. These methods have brought results of considerable interest in ventilation ducts [6], vehicles [7], [8], open spaces [9], [10], and industrial plants [11].

First proposed by Lueg [12], ANC is based on the principle of destructive interference. It exploits an electromechanical or electroacoustic device to generate an anti-noise of equal amplitude and opposite phase of the primary noise source so that they cancel each other [13]. Typically, these systems use adaptive filters [14], [15] to address challenges associated with the non-stationarity of frequencies, amplitudes, phases, and speed of sound. ANC systems can be classified into

The associate editor coordinating the review of this manuscript and approving it for publication was Hassen Ouakad [].

feed-forward [16] and feedback control [17] algorithms. In feed-forward control, the system detects coherent reference noise before it reaches the receiver, while feedback control does not involve a reference input. Additionally, ANC systems can be classified as broadband adaptive control when the algorithm operates over a wide range of frequencies, and narrowband adaptive control when it focuses on a limited number of harmonics. As an esteemed adaptive feed-forward algorithm for ANC, the Filtered-x Least Mean Square (FxLMS) has found extensive application due to its low computational cost and compact structure [18], [19].

Acoustics ANC systems suffer from some limitations in outdoor applications. The presence of a microphone as an error sensor may be impractical due to the presence of the cable that connects the microphone to the control unit. In the case of a cogenerator plant, which is the problem addressed in this work, there are cultivated fields around the cogenerator, which makes it not possible to install a permanent error microphone. Moreover, the microphone must be positioned at a great distance from the noise source, so that the sound wave resembles a plane wave, ensuring that the cancellation is not punctual, but remains effective even at greater distances. Furthermore, in outdoor applications the ageing of the loudspeakers employed as controlling devices is another problem, due to the presence of humidity, significative temperature variations, rain, and dust, as referred in [20].

Other limitations in practical implementation of most ANC systems comes from the electronic boards that run the algorithm in real-time. An existing solution based on the ADAU1466Z evaluation board by Analog Devices was tested, which integrates a FxLMS cancellation module. Although a hardware-in-the-loop laboratory test showed promising results [11], the system failed to provide effective cancellation in a real-life scenario. In this case, the evaluation board failed to calculate consistent secondary paths, as it relies on the white noise signal, which is not powerful enough to ensure a sufficient signal-to-noise ratio (SNR). The ADAU1466Z also has a limited number of inputs (4) and outputs (8), allowing only these configurations: 1-3-8, 2-2-8, 3-1-8 (first number indicates the reference signals, the second number indicates the error signals, the third number indicates the control signals).

For the reasons stated above, in this work an active vibration control (AVC) system has been developed, aimed at reducing noise by attenuating the vibration that causes it. The error microphone is replaced by an accelerometer mounted directly on the cogenerator enclosure, and the control loudspeakers are replaced by electrodynamic shakers. This solution avoids the need for a long wire connecting the error microphone to the control unit, and the entire system is self-contained in the cogenerator enclosure. Electrodynamic shakers are suitable for an outdoor application, being more resistant than loudspeakers to environmental conditions, due to the absence of the membrane and suspensions. In the

proposed solution, waterproof (IP68) shakers were employed. The system uses the FxLMS algorithm, implemented in the form of a Virtual Studio Technology (VST) plugin, so it can run in real-time in any Digital Audio Workstation (DAW) installed on a regular laptop or personal computer (PC). This solution is practical for several reasons: a PC is already present in the control room next to the cogenerator plant, and the possible configurations of the system are independent from the hardware, which can be chosen based on the needs of the application. Furthermore, the developed VST plugin makes use of the Exponential Sine Sweep (ESS) technique [21], a solution that allowed us to correctly measure the secondary paths required by the ANC algorithm, as it guarantees an increase of the SNR of tens of dB.

The paper is organized as follows: Section II provides theoretical overviews of ANC algorithms; Section III describes the equipment and sensors used for the experimental measurements; Section IV presents the experimental characterization of cogenerator noise and vibration; the VST implementation of the algorithm is described in Section V; Section VI describes the laboratory validation of the developed technique; Section VII presents the results obtained on the cogenerator, underlining the main advantages and limitations of the proposed solution, and, finally, Section VIII summarizes the conclusions.

II. RECALL ON ACTIVE NOISE CONTROL ALGORITHM

This section provides a concise overview of the theoretical basis of ANC and the algorithm used to implement it.

A. THEORETICAL CANCELLATION

ANC systems work on the principle of destructive interference. Let us initially consider a system comprising only an error transducer. The theoretical maximum cancellation can be expressed as follows:

$$y + (-y') = e \tag{1}$$

where e represents the residual noise, y indicates the error signal, and y' is the noise measured at the error sensor and coherent with the reference signal x. The coherent noise component y' is obtained through a linear convolution:

$$y' = x * h \tag{2}$$

where x denotes the reference signal and h is the time domain version of the transfer function H_1 between the reference signal x and the error signal y. The transfer function $H_1(f)$ can be calculated as:

$$H_1(f) = \frac{P_{yx}(f)}{P_{xx}(f)} \tag{3}$$

where f denotes the frequency, P_{yx} represents the Cross Power Spectral Density (CPSD) between the input signal x and the output signal y, and P_{xx} is the Power Spectral Density (PSD) of the input signal x. The time domain transfer function h can be obtained by applying the Inverse Fast Fourier Transform (IFFT).

B. FxLMS

FIGURE 1 illustrates the block diagram of the FxLMS algorithm. $P(z)$ and $S(z)$ indicate the primary and secondary paths, respectively. The primary path represents the transfer function between the noise signal and the error signal, while the secondary path represents the transfer function between the actuator (e.g., a shaker or loudspeaker) and the error sensor. $W(z)$ denotes the adaptive filter, which adjusts its coefficients $w(n)$ to minimize the instantaneous squared error $\hat{\xi} = e^2(n)$ by matching the primary path, using the steepest descent algorithm:

$$w(n+1) = w(n) + \mu x'(n) e(n) \qquad (4)$$

where μ is the step size, $x'(n) = \hat{s}(n) * x(n)$, and $\hat{s}(n)$ is the estimate of $s(n)$. During an initial training phase in most ANC applications, secondary path $\hat{s}(n)$ estimation is performed to obtain an accurate model. The error $e(n)$ is calculated as follows:
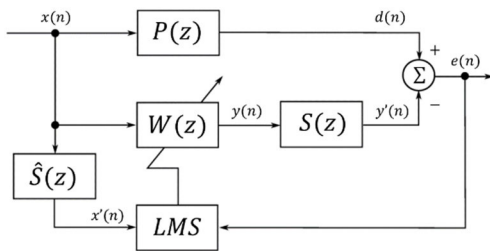
$$e(n) = d(n) - s(n) * [w(n) x(n)] \qquad (5)$$

FIGURE 1. Schematic of a FxLMS algorithm.

Here, n represents the discrete time index, $d(n)$ denotes the primary disturbance, $s(n)$ denotes the coefficients of the secondary path $S(z)$, and $*$ denotes the linear convolution. Furthermore:

$$x(n) = [x(n) x(n-1) \ldots x(n-L+1)]^T \qquad (6)$$

denotes the input signal vectors, where L is the filter order. The coefficient μ used in (4) requires careful tuning for each specific application. Typically, this optimization process is performed manually, with the goal of optimizing the effectiveness and speed of convergence of the algorithm (higher values of the step size) while reducing the instability of the system (lower values of the step size). Since disturbances in the reference signal can potentially lead to system instability, a common approach is to use the normalized FxLMS algorithm (FxNLMS). In this method, the variable step size [21] is adjusted dynamically by weighting it proportionally to reference signal power, as expressed by:

$$\mu = \frac{\beta}{x'^T(n) x'(n)} \qquad (7)$$

where β is a constant, theoretically comprised between 0 and 2, but the practical recommended choice is $0 < \beta < 1$ [22]. This adjustment ensures that the step size

adapts to variations in the reference signal power, improving the stability and performance of the ANC system under different operating conditions. In our case, the value of β was set to 0.1 as suggested in [23], to ensure system stability while maintaining a good convergence speed and performance.

III. MATERIAL AND EQUIPMENT

Several measurements were performed to validate, optimize, and evaluate the effectiveness of the developed technique. This section describes the equipment and sensors employed, providing their technical specifications.

The audio interface used in the experimental measurements for signal collection and transmission was a Roland Studio Capture (see Table 1), due to the availability of 8-line outputs and its capability to operate stably with a total latency of just 1.33 ms, calculated as follows:

$$l = \frac{2 \cdot B_s}{f_s} \qquad (8)$$

where $B_s = 32\ samples$ is the buffer size and $f_s = 48\ kHz$ the standard sampling frequency in current audio applications. Coefficient 2 is required to consider both the input and the output buffers.

TABLE 1. Roland studio capture audio interface.

Specification	Value
Number of analog inputs/outputs	12 / 12
Connection	USB 2.0
Analog input power supply	Yes, phantom 48 V
Input dynamic range	105 dB
Output dynamic range	114 dB
Sampling frequency	48 kHz
Buffer size	32 samples
Resolution	24 bits

The sensors employed were PCB Piezotronics type 333B30 accelerometers (single axis, sensitivity 100 mV/g, full scale ±50 g) and Bruel&Kjaer (B&K) microphones type 4189 (sensitivity 50 mV/Pa) with preamplifier type 1706. The specifications are shown in Table 2 (accelerometer) and Table 3 (microphone). The accelerometers were used as reference and error transducers, while the microphones were used to characterize the acoustic noise emission of the cogenerator and to perform a modal analysis on the cogenerator enclosure to define the optimal positions of the control transducers.

Eight electrodynamic shakers from Monacor, type AR-50, having a nominal power of 30 Wrms and an impedance of 8 Ω were used as control devices. They were driven by an analog amplifier, QSC CX168, connected to the audio interface outputs. The specifications of the shakers and amplifier are shown in Table 4 and Table 5, respectively.

Finally, a B&K impact hammer, the specifications of which are shown in Table 6, was employed to perform the

TABLE 2. Accelerometer PCB piezotronics 333B30.

Specification	Value
Sensitivity (± 10%)	100 mV/g
Measurement range	±50 g
Frequency range (+/-5 %)	$0.5 - 3000$ Hz
Broadband resolution	0.00015 g rms*
Operating temp. range	-18 °C to +66 °C
Excitation voltage	$18 - 30$ VDC
Spectral noise (1 Hz)	39 μg/√Hz
Spectral noise (10 Hz)	11 μg/√Hz
Spectral noise (100 Hz)	3.4 μg/√Hz
Spectral noise (1 kHz)	1.4 μg/√Hz

* Root Mean Square (RMS)

TABLE 3. Microphone and preamplifier Bruel&Kjaer 4189-1706.

Specification	Value
Diameter	½ inch
Self-noise	15.2 dB(A)
Sensitivity	50 mV/Pa

TABLE 4. Electrodynamic shaker monacor AR-50.

Specification	Value
Impedance	8 Ω
Resonant frequency	500 Hz
Power rating	30 Wrms
Power output max	50 W peak
Protective class	IP68
Operating temperature range	-30 °C to +40 °C
Weight	0.975 kg

TABLE 5. Power amplifier QSC CX168.

Specification	Value
Power rating	90 Wrms at 8 Ω, 0.05% THD
Number of outputs channels	8
Class	AB
Signal to Noise (20 Hz − 20 kHz)	-107 dB
Voltage gain	x20 (26 dB)
Freq. response (20 Hz – 20 kHz)	+ 0.2 dB

TABLE 6. Impact hammer Bruel&Kjaer 8206.

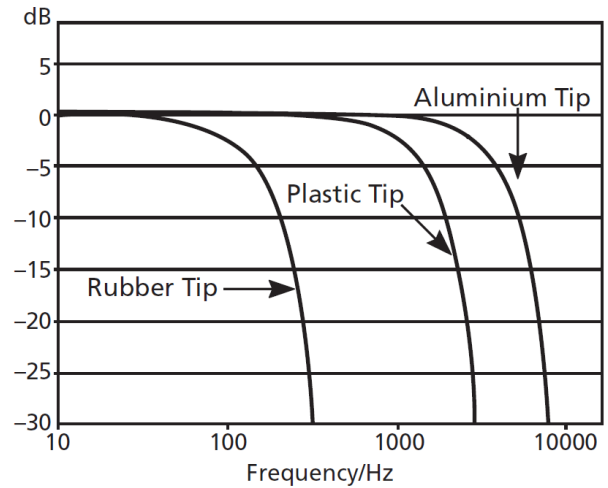| Specification	Value
Head mass	100 g
Sensitivity	22.5 mV/N
Range full scale	222 N
Maximum force	4448 N

FIGURE 2. Frequency responses of the B&K impact hammer for rubber, plastic, and aluminum tips.

IV. VIBRATIONAL AND ACOUSTIC ANALYSIS OF THE COGENERATOR

The measurements carried out on the cogenerator to obtain a complete acoustic and vibrational study are presented here.

A. COGENERATOR NOISE CHARACTERIZATION

The cogenerator engine is housed inside a metal enclosure three meters wide, nine meters long, and three meters high. The sound field produced by the system can be assumed as a free field, as the cogenerator is positioned outside, in an open environment, without any reflective barrier at close range, on flat grassy ground.

First, the acoustic characterization of the noise produced by the plant was carried out, positioning a B&K microphone in front of the long side of the cogenerator, at 2 m height and at an increasing distance of 10 m, 20 m, and 40 m. Furthermore, the background noise was also measured at 10 m distance with the cogenerator turned off. FIGURE 3 illustrates the Sound Pressure Level (SPL) spectra of recorded noise, over the frequency range $50 - 250$ Hz, which is the range where the most significant noise reduction can be achieved. The spectra were obtained by averaging multiple Fast Fourier Transform (FFT) blocks, each consisting of 2^{14} samples, overlapping by 75 %, and using a Hann window function. Therefore, the frequency resolution is $df = f_s/2^{14} \cong 2.9 Hz$, where $f_s = 48\ kHz$ is the sampling frequency of the sound card. A reduction of 6 dB can be seen for each doubling of distance in the frequency range from 55 Hz to 80 Hz, which is the

modal analysis aimed at identifying the optimal positions of the shakers to maximize the effectiveness of the system. The frequency range of the impact hammer is influenced by the material of the tip mounted on its top (FIGURE 2). Since the maximum operating frequency of the AVC system under development is less than 250 Hz, it was chosen to use the rubber tip, which provides energy up to 300 Hz, without damaging the cogenerator enclosure (as happens with the aluminum tip) or suffer damage by impacts (as with the plastic tip).

decay expected for an ideal point source (acoustic monopole) radiating spherical waves in free field. Three main frequency components are detected at 100 Hz, 112.5 Hz, and 125 Hz, at which the main cancellation effect is therefore desirable. Above 145 Hz, most of the energy is dissipated at 40 m distance. The 90 Hz and 180 Hz tonal components can be found both with the cogenerator on and off, therefore they can be addressed to environmental noise not strictly linked to the cogenerator system.
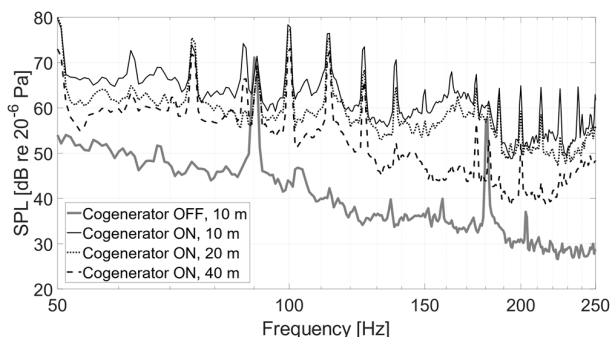

FIGURE 3. SPL spectra of environmental background noise at 10 m distance (solid gray line) and of cogenerator noise at 10 m (solid black line), 20 m (dotted line), and 40 m (dashed line) distances, measured with the B&K 4189 microphone.

B. POSITIONING OF CONTROL TRANSDUCERS

The position of the controllers (i.e., the shakers) is a crucial aspect to maximize the cancellation performance, and for this reason it has been carefully analyzed. A modal analysis was performed on the wall of the cogenerator enclosure where the control shakers will be installed in the real application. A measurement campaign was carried out with the B&K impact hammer (see Table 6) and three B&K microphones (see Table 3) positioned in front of the wall under test, at 3 m distance. A schematic of the measurement is shown in FIGURE 4.
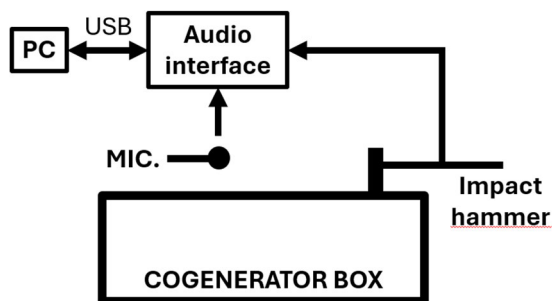

FIGURE 4. Schematic of the impact hammer measurement for modal analysis.

A total of 54 points were tested, arranged at three different heights (0.65 m, 1.30 m, 1.95 m) and spaced horizontally by 0.63 m. For each point, 5 impacts were recorded, waiting at least 10 s between one impact and the next, to ensure the complete extinction of the vibration. The analysis was

performed by calculating the transfer function H_1 between the hammer load cell as the input signal x and the microphones as the output signals y (see (3) in Section II). The optimal locations for eight control transducers were selected as those that show the maximum energy in the relevant frequency range, i.e. 50-250 Hz, meaning that those points can radiate the maximum amount of energy. A picture of the tested enclosure (with the three microphones in front of it) is shown in FIGURE 5 (top), while all the tested points can be seen in FIGURE 5 (bottom). Positions identified as optimal are highlighted by a red circle.

FIGURE 5. Tested cogenerator enclosure (top) and measured points with impact hammer for modal analysis (bottom). Optimal positions are highlighted with a red circle.

C. SECONDARY PATH MEASUREMENT

The secondary path represents the transfer function between the control devices K and the error transducers M. In the presented application, one error signal and eight control devices were used, therefore M = 1 and K = 8.

The measurements were carried out with the system turned off, one shaker at a time. The ESS technique [24] was employed because it allows separating the linear response from the high-order harmonic distortion components and provides an increase in SNR of tens of dB. Each shaker was excited with an ESS signal of 10 s length in the frequency range 10 Hz – 1 kHz with an output voltage of 10 Vrms, measured under load at the amplifier terminals with a true-RMS tester. Then, the recorded signals were convolved with the inverse ESS to obtain the time-domain Impulse Responses (IRs) between each shaker and the error accelerometer. Finally, the linear part of the IRs was cut and windowed. A schematic of the measurement is shown in FIGURE 6.

D. POSITIONING OF ERROR AND REFERENCE SENSORS

Following the manufacturer's suggestions, the error accelerometer was installed at the mid-height of the cogenerator housing, in correspondence of the midpoint of the engine positioned behind (see the red circle in FIGURE 16), being the position more correlated with the primary noise source (the cogenerator engine). The reference accelerometer was installed on the engine crankcase (FIGURE 7) to avoid the feedback caused by the controllers (the shakers mounted
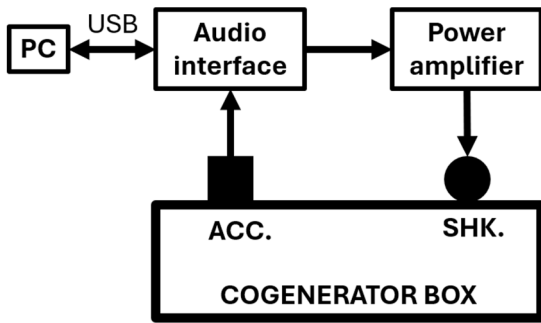
FIGURE 6. Secondary path measurement scheme.

on the cogenerator enclosure) which act on the reference sensor. A crosstalk analysis was performed to assess whether the crankcase and the enclosure are sufficiently decoupled, thus limiting the detrimental effect of the feedback. An ESS signal was reproduced by one of the shakers and recorded simultaneously with the reference (engine crankcase) and the error (cogenerator enclosure). After convolution, linear IR spectra were calculated, allowing to assess that the crosstalk produced by the shaker on the reference sensor is at least 30 dB lower than the error sensor across the entire frequency range of interest. An ANC solution with feedback compensation can be found in [25], and it will be evaluated in the future.
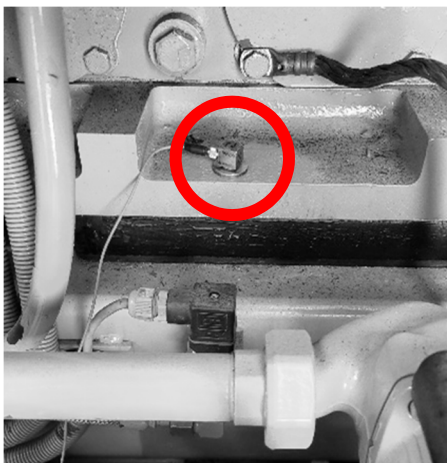

FIGURE 7. Reference accelerometer mounted on the cogenerator engine crankcase.

Then, a two-minutes recording was made simultaneously with both sensors and the cogenerator turned on. In FIGURE 8, the acceleration spectra are shown, obtained with the previously described procedure and settings. The three main frequencies produced by the cogenerator engine (solid line), which were already observed in the acoustic noise spectra of FIGURE 3, can be seen at 100 Hz, 112.5 Hz, and 125 Hz. They are also visible on the cogenerator enclosure (dashed line), for which the 100 Hz and 112.5 Hz components are the

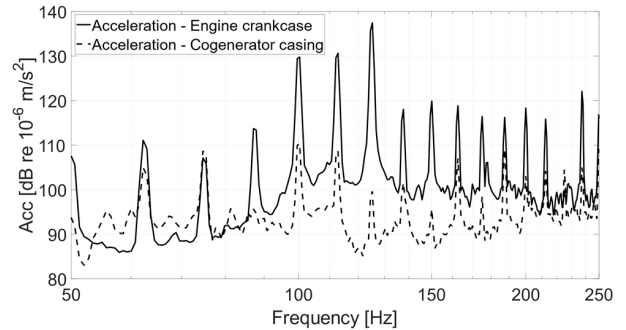most energetic, while the component at 125 Hz has a lower amplitude.

FIGURE 8. Acceleration spectra on cogenerator engine crankcase (solid line) and cogenerator enclosure (dashed line).

V. VST PLUGIN DEVELOPMENT

The VST plugin solution allows to use the FxNLMS algorithm in real-time in any DAW without the need to implement it with a low-level language on a Digital Signal Processing (DSP) unit. The algorithm was implemented in a Multi-Input Multi-Output (MIMO) configuration up to 8-8-8, although a Single-Input Multi-Output (SIMO) configuration of type 1-1-8 was used for the practical application. The implementation was carried out using the MATLAB platform, more specifically relying on the Audio Toolbox. An overview of the plugin control window is shown in FIGURE 9, where the main parameters can be seen: down sampling factor, step-size μ, length of the filter $W(z)$. The software works in two modes: *Secondary Path* and *Real-time Cancelling*. In this section the general operating principle of the VST plugin will be described, with reference to the technical characteristic implemented.

FIGURE 9. Main control window of the VST plugin.

A. SECONDARY PATH MODE

The plugin incorporates a *'Secondary Path mode'*, which allows secondary path calculation as described in section IV, subsection D. FIGURE 10 shows the signal path in a configuration with four control actuators. At startup, an ESS with the corresponding inverse filter is generated and stored. The ESS covers the frequency range from 10 Hz to 1 kHz and lasts

for 10 seconds, at a sampling frequency of 48 kHz. The signal is emitted on each output channel, one at a time, recorded by the error transducers, and convolved with the inverse filter to obtain the IRs, the linear part of which is selected and windowed. Since the entire procedure is fast thanks to the use of the ESS, it can be scheduled periodically, allowing to maintain the secondary path constantly updated. This ensures consistent performance over time [26], making the system independent from the ageing of both the cogenerator enclosure and the shakers. It also takes into account variations in air temperature and humidity as well as different boundary conditions, such as the presence of objects, vehicles (cars and agricultural machinery), cultivated or plowed land.

FIGURE 10. Signal path diagram in the DAW for the Secondary Path mode of the VST plugin.

In FIGURE 10, two anti-aliasing blocks can also be seen immediately before and after the plugin. It was chosen not to include them in the plugin to reduce the computational load. The anti-aliasing filters were replaced with precalculated Finite Impulse Response (FIR) filters and two efficient matrix convolvers [27]. Butterworth low-pass filters were used, with a cut-off frequency of 500 Hz and an order of 20.

B. AVC MODE

After calculating the secondary paths, the plugin can switch to *Real-time Cancelling* mode. As an example, FIGURE 11 shows the signal path for a 2-1-4 configuration (2 reference, 1 error and 4 control signals). The two reference signals x_1, x_2 and the error signal e_s pass through the anti-aliasing filter obtaining x_1', x_2' and e_s' respectively. After filtering, all these signals are passed to the down sampling block, together with the previously calculated secondary path S_e, resulting in signals at a sampling frequency equal to:

$$f_s' = \frac{f_s}{D} \qquad (9)$$

where f_s is the sampling frequency (48 kHz) and D is the down sampling factor, chosen between 1 (no down sampling) and a power of two. The obtained signals are then fed into the FxNLMS algorithm block, which calculates the control signals as described in Section II. Finally, the control signals are up sampled by the same factor D and passed through the anti-aliasing filter, resulting in the final signals delivered to the actuators. The last two parameters in the plugin, the "Save filter" and "Reset" checkboxes, allow to save the

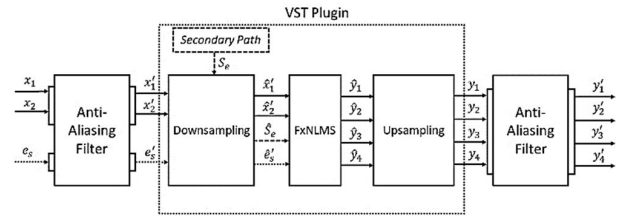filter coefficients of $W(z)$ to a text file or reset them to zero, respectively.

FIGURE 11. Signal path diagram for the Real-time Cancelling mode of the VST plugin.

VI. LABORATORY VALIDATION

A laboratory test was performed to evaluate the effectiveness of the algorithmic implementation. A "dummy" shaker positioned on the ground was used to artificially create a disturbing vibration, thus replacing the cogenerator. This signal was then captured by a reference accelerometer also positioned on the ground. A second shaker, the controller, was installed on a desk, where a second accelerometer was placed to measure the error signal. Therefore, the system configuration is 1-1-1. An image of the experiment is shown in FIGURE 12, while a schematic is depicted in FIGURE 13.
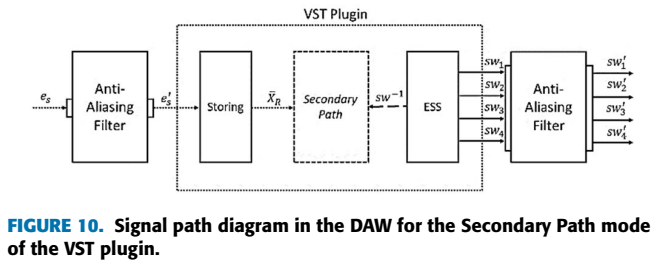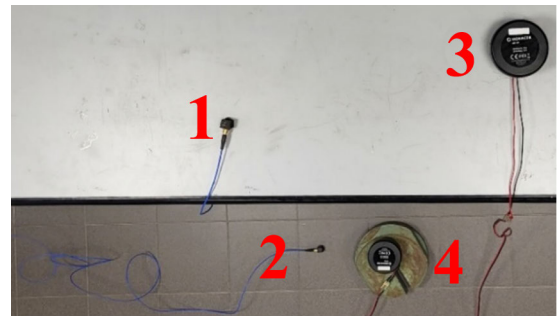
FIGURE 12. An image of the laboratory experiment performed to validate the VST implementation of the AVC algorithm. In order: 1. error accelerometer, 2. reference accelerometer, 3. control shaker, 4. disturbing shaker.
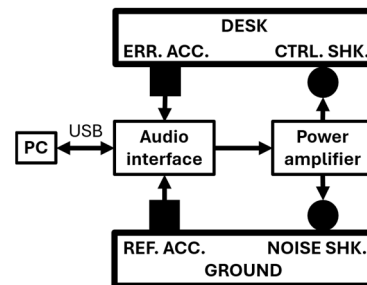
FIGURE 13. Schematic of the laboratory experiment performed to validate the VST implementation of the AVC algorithm.

Two repetitions of the experiments were performed, first feeding the disturbing shaker (4 in FIGURE 12) with a pure

tone at 100 Hz, then with white noise. In each case, a 2-minute recording of the error accelerometer (1 in FIGURE 12) was made, starting with the AVC algorithm turned on and then turned off (this can easily be achieved by bypassing the VST plugin in the DAW). FIGURE 14 shows a 20-second portion of the time domain recordings for the pure tone (above) and the white noise (below). The RMS values of the acceleration on the error sensor were calculated for the AVC on and off conditions and the results are summarized in Table 7. The algorithm proved to be highly effective, as the rms value was reduced by a factor 22.7 in the case of pure tone at 100 Hz and by a factor 1.7 in the case of white noise.
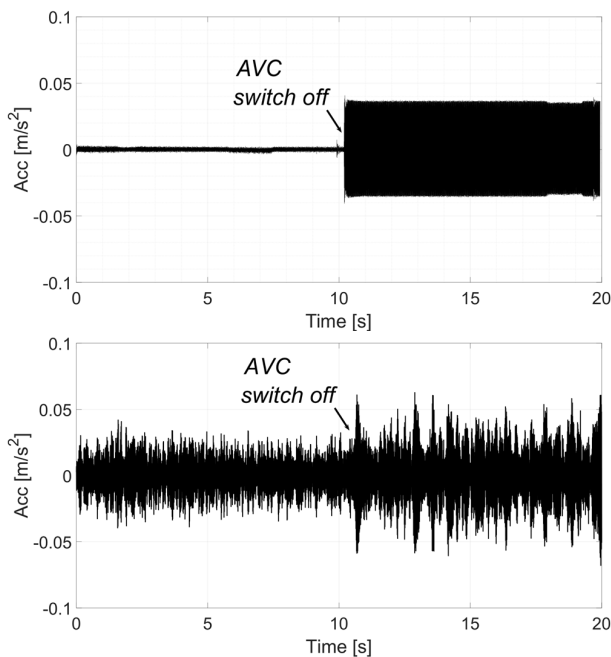

FIGURE 14. Time domain recordings of the laboratory test for the AVC on/off conditions. Single tone (above), white noise (below).

TABLE 7. Results in time domain of the laboratory validation test.

Type of signal	AVC condition	Acceleration $[m/s^2\ rms]$
Pure tone at 100 Hz	ON	0.0011
Pure tone at 100 Hz	OFF	0.025
White noise	ON	0.0116
White noise	OFF	0.0197

In FIGURE 15, the spectra of the AVC on and off conditions are compared for the pure tone (above) and the white noise (below). With pure tone an attenuation of up to 34.3 dB was obtained, while up to 14.6 dB with white noise in the frequency range 86-96 Hz.

VII. EXPERIMENTAL RESULTS

Eventually, the developed system was installed on the cogenerator, located in the production site of Galliavola,
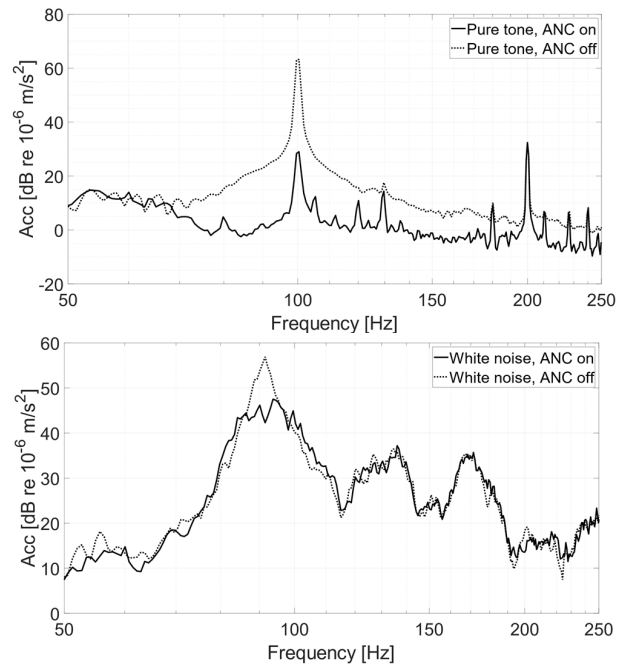

FIGURE 15. Acceleration spectra of the laboratory test for the AVC on/off conditions. Single tone (above), white noise (below).

Pavia (Italy). The system configuration is 1-1-8, with one reference, one error and eight control signals. The positions of the reference and error accelerometers were already discussed in Section IV, subsection D. It was not possible to install the control shakers in the optimal locations presented in Section IV, subsection B (FIGURE 5), because the enclosure was significantly different from the one analyzed. The actual positions of the shakers can be seen in FIGURE 16. At the same time, this allows us to demonstrate the versatility of the system, which worked correctly even for shaker positions other than the optimal ones.

FIGURE 16. A picture of the cogenerator with the eight control shakers (numbered) and the error accelerometer (highlighted with a red circle) installed.

In this case, numerous measurements were carried out turning the AVC on and off, with different values of the step-size parameter, with the aim of experimentally optimizing the convergence speed, cancellation effectiveness and system

stability. The step size parameter was varied in steps of 0.001 from 0.001 to 0.01. At the end of this procedure, the step size μ was set to 0.005. In FIGURE 17, the spectra of the AVC on and off conditions are compared for $\mu = 0.005$, and the attenuation results are summarized in Table 8. The authors have made these data publicly available on IEEE Dataport [28].
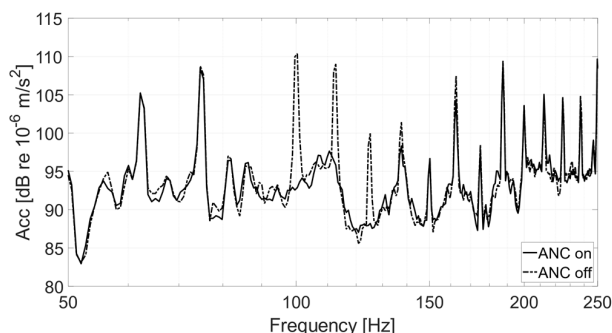

FIGURE 17. Comparison of the acceleration spectra at the error sensor between on and off conditions for the final system installed on the cogenerator.

TABLE 8. Results in frequency domain of the AVC system installed on the cogenerator plant.

Frequency [Hz]	Attenuation [dB]
100.0	-17.5
112.5	-13.2
125.0	-11.8
137.7	-3.1
162.6	-3.1

It can be seen that the two lowest frequency components, 62.5 Hz and 75 Hz, were not attenuated. This behavior can be traced back to the limited efficiency of the shakers at low frequency. In the future, a larger, heavier and more powerful shaker will be used or designed, reducing the number and improving the performance towards low frequencies. Despite this, the AVC system has proven effective in attenuating numerous harmonics in the range 100 Hz – 162.6 Hz. At the same time, the effectiveness was limited only to the most energetic frequencies contained in the primary signal. This constrain could be overcome by adopting a Frequency-Domain FxLMS [29] algorithm. However, such a solution is more demanding in terms of computational load, and it would not be feasible with the current VST compilation method, which makes use of high-level software (MATLAB). Therefore, the algorithm will be rewritten natively in a low-level language (e.g., C++), in a specific framework for VST development (e.g., JUCE). Otherwise, since the signal to be attenuated is predominantly tonal, a multi-tone ANC algorithm [30] could be adopted, less computationally demanding than the FxLMS, as referred in [31]. Finally, this improvement in computational cost could allow for a configuration based on multiple error accelerometers

positioned at various points of the cogenerator shell. Given the large size of the cogenerator wall, this approach could be particularly advantageous, allowing noise cancellation to be distributed over the entire structure instead of focusing on a single area.

VIII. CONCLUSION

An effective implementation of an active vibration control system aimed at noise reduction of a cogeneration plant was presented. The proposed solution uses electrodynamic shakers and accelerometers and offers significant advantages compared to traditional systems, which rely on loudspeakers and microphones. The latter require cables, which are not practical in our application, while special loudspeakers and installation designs are required for continuous, long-term outdoor use.

The cogeneration plant was first characterized from both a vibrational and acoustic point of view, allowing us to determine the main frequency components of the acoustic disturbance, the optimal positions of the shakers, and the secondary paths required by algorithm, namely the FxNLMS. The algorithm was implemented in a VST plugin, which runs in real-time on a PC. This solution separates the software from the hardware, allowing us to choose the equipment (sound card, amplifiers) based on the specific application and overcome the limitations normally present in the hardware currently available on the market. Prior to real-world application, the plugin was validated in a laboratory test, demonstrating attenuation of -34.3 dB on a single tone and of -14.6 dB on white noise. Finally, the system was installed on the cogenerator, and allowed five frequencies to be significantly attenuated: -17.5 dB at 100 Hz, - 13.2 dB at 112.5 Hz, -11.8 dB at 125 Hz, -3.1 dB at 137.7 Hz, and -3.1 dB at 162.6 Hz.

Although the system performed well in real-world conditions, it showed some limitations and offers opportunities for improvement. At present, many small shakers are used, while the design of a specific shaker would allow their number to be reduced and performance to be improved, particularly below 100 Hz, where the current shaker is not effective. The algorithm was implemented in MATLAB, making development quick and easy. However, rewriting the plugin natively in a low-level language, e.g. C++, would allow to test more effective, but also complex and computationally demanding algorithms, such as the Frequency-Domain FxNLMS. Finally, since the noise to be attenuated is mainly tonal, other multi-tone ANC algorithms may prove effective.

REFERENCES

[1] E. Peris, "Environmental noise in Europe: 2020," *Eur. Environ. Agency*, vol. 1, p. 104, Aug. 2020.

[2] *Environmental Noise Guidelines for the European Region*, World Health Org., Geneva, Switzerland, 2018.

[3] C. M. Harris, *Handbook of Acoustical Measurements and Noise Control*. New York, NY, USA: McGraw-Hill, 1991.

[4] L. L. Beranek and I. L. Ver, *Engineering Sound and Vibration Control. Principles and Applications*. Hoboken, NJ, USA: Wiley, 1992.

[5] B. Widrow, J. R. Glover, J. M. McCool, J. Kaunitz, C. S. Williams, R. H. Hearn, J. R. Zeidler, J. Eugene Dong, and R. C. Goodlin, "Adaptive noise cancelling: Principles and applications," *Proc. IEEE*, vol. 63, no. 12, pp. 1692–1716, 1975, doi: 10.1109/proc.1975.10036.

[6] C.-N. Wang, C.-C. Tse, and C.-W. Wen, "A study of active noise cancellation in ducts," *Mech. Syst. Signal Process.*, vol. 11, no. 6, pp. 779–790, Nov. 1997, doi: 10.1006/mssp.1997.0111.

[7] W. Jung, S. J. Elliott, and J. Cheer, "Local active control of road noise inside a vehicle," *Mech. Syst. Signal Process.*, vol. 121, pp. 144–157, Apr. 2019, doi: 10.1016/j.ymssp.2018.11.003.

[8] C. Belicchi, A. Opinto, M. Martalo, A. Tira, D. Pinardi, A. Farina, and G. Ferrari, "ANC: A low-cost implementation perspective," in *Proc. SAE Tech. Papers*, 2022, pp. 1–8, doi: 10.4271/2022-01-0967.

[9] J. Zhang, T. D. Abhayapala, W. Zhang, P. N. Samarasinghe, and S. Jiang, "Active noise control over space: A wave domain approach," *IEEE/ACM Trans. Audio, Speech, Language Process.*, vol. 26, no. 4, pp. 774–786, Apr. 2018, doi: 10.1109/TASLP.2018.2795756.

[10] H. Huang, X. Qiu, and J. Kang, "Active noise attenuation in ventilation windows," *J. Acoust. Soc. Amer.*, vol. 130, no. 1, pp. 176–188, Jul. 2011, doi: 10.1121/1.3596457.

[11] E. Voltolini, D. Pinardi, A. Toscani, M. Binelli, A. Farina, J. Ferrari, S. Maglia, A. Zenaro, and E. Calzavacca, "Design of an active noise reduction system for a cogeneration plant," in *Proc. Immersive 3D Audio, From Archit. Automot. (I3DA)*, 2023, pp. 1–7.

[12] P. Lueg, "Process of silencing sound oscillations," U.S. Patent 2 043 416, Jun. 9, 1936.

[13] P. A. Nelson and S. J. Elliott, *Active Control of Sound*. New York, NY, USA: Academic, 1991.

[14] B. Widrow and S. D. Stearns, *Adaptive Signal Processing*. Englewood Cliffs, NJ, USA: Prentice-Hall, 1985.

[15] S. Haykin and B. Widrow, *Least-Mean-Square Adaptive Filters*. New York, NY, USA: Wiley, 2003.

[16] S. M. Kuo and J. Tsai, "Acoustical mechanisms and performance of various active duct noise control systems," *Appl. Acoust.*, vol. 41, no. 1, pp. 81–91, 1994.

[17] H. F. Olson and E. G. May, "Electronic sound absorber," *J. Acoust. Soc. Amer.*, vol. 25, no. 4, pp. 1–829, Jul. 1953.

[18] E. Bjarnason, "Analysis of the filtered-X LMS algorithm," *IEEE Trans. Speech Audio Process.*, vol. 3, no. 6, pp. 504–514, Jul. 1995, doi: 10.1109/89.482218.

[19] D. R. Morgan, "History, applications, and subsequent development of the FXLMS algorithm [DSP history]," *IEEE Signal Process. Mag.*, vol. 30, no. 3, pp. 172–176, May 2013, doi: 10.1109/MSP.2013.2242394.

[20] W. Klippel, "Modeling and testing of loudspeakers used in sound-field control," in *Advances in Fundamental and Applied Research on Spatial Audio*. IntechOpen, 2022, doi: 10.5772/intechopen.102029.

[21] R. H. Kwong and E. W. Johnston, "A variable step size LMS algorithm," *IEEE Trans. Signal Process.*, vol. 40, no. 7, pp. 1633–1642, Jul. 1992, doi: 10.1109/78.143435.

[22] H. Yiteng, *Adaptive Signal Processing—Applications to Real-World Problems*. Berlin, Heidelberg: Springer, 2003, doi: 10.1007/978-3-662-11028-7.

[23] A.-G. Rusu, C. Paleologu, J. Benesty, and S. Ciochina, "A variable step size normalized least-mean-square algorithm based on data reuse," *Algorithms*, vol. 15, no. 4, p. 111, Mar. 2022, doi: 10.3390/a15040111.

[24] A. Farina, "Simultaneous measurement of impulse response and distortion with a swept-sine technique," in *Proc. 108th Conv., Paris, France*, 2000, pp. 1–24.

[25] S. M. Kuo and D. R. Morgan, "Active noise control: A tutorial review," *Proc. IEEE*, vol. 87, no. 6, pp. 943–975, Jun. 1999, doi: 10.1109/5.763310.

[26] J. Y. Oh, H. W. Jung, M. H. Lee, K. H. Lee, and Y. J. Kang, "Enhancing active noise control of road noise using deep neural network to update secondary path estimate in real time," *Mech. Syst. Signal Process.*, vol. 206, Jan. 2024, Art. no. 110940, doi: 10.1016/j.ymssp.2023.110940.

[27] A. Farina. *X-MCFX Convolver*. Accessed: Apr. 30, 2024. [Online]. Available: http://www.angelofarina.it/X-MCFX.htm

[28] A. Toscani, E. Voltolini, D. Pinardi, M. Binelli, A. Farina, J. Ferrari, S. Maglia, A. Zenaro, and E. Calzavacca, "Noise and vibration measurements on a cogenerator plant," IEEE Dataport, 2024, doi: 10.21227/wv3e-a206.

[29] F. Yang, Y. Cao, M. Wu, F. Albu, and J. Yang, "Frequency-domain filtered-X LMS algorithms for active noise control: A review and new insights," *Appl. Sci.*, vol. 8, no. 11, p. 2313, Nov. 2018, doi: 10.3390/app8112313.

[30] S. Kim and Y. Park, "Active control of multi-tonal noise with reference generator based on on-line frequency estimation," *J. Sound Vibrat.*, vol. 227, no. 3, pp. 647–666, Oct. 1999, doi: 10.1006/jsvi.1999.2383.

[31] F. P. Ribeiro and V. H. Nascimento, "A robust and computationally efficient method for tonal active noise control using a simplified secondary path model," in *Proc. IEEE Int. Conf. Acoust., Speech Signal Process.*, Mar. 2008, pp. 345–348, doi: 10.1109/ICASSP.2008.4517617.

EMANUELE VOLTOLINI received the B.S. degree in automation engineering and the M.S. degree in music and acoustic engineering from the Politecnico di Milan, Italy, in 2019 and October 2022, respectively, with a thesis on deep learning applied to acoustic guitar pick-up—microphone sound modeling.

From January 2023 to November 2023, he was a Research Fellow with the University of Parma on active noise control. Since November 2023, he has been involved in a Ph.D. study on predictive maintenance with the University of Parma.

DANIEL PINARDI received the M.S. degree (cum laude) in mechanical engineering from the University of Parma, Italy, in July 2016, with a thesis on loudspeaker modeling and the Ph.D. degree (Doctor Europaeus) in industrial engineering from the University of Parma, in March 2020, with a thesis on the design of microphone, hydrophone, and camera arrays for spatial audio and video recording.

He has been a Research Assistant of Prof. Angelo Farina with the University of Parma, since 2016, specialized in spatial audio, design of transducer arrays, acoustics simulations and 3D auralization, applied to automotive field, and underwater acoustics.

ANDREA TOSCANI received the M.S. degree (cum laude) in electronic engineering and the Ph.D. degree in information technology from the University of Parma, Italy, in 2004 and 2008, respectively.

Since 2004, he has been with the Department of Engineering and Architecture, University of Parma, where he is currently a Research Fellow. His research interests include power electronics, high-performance electric drives for various industrial and consumer applications, diagnostic techniques for industrial electric systems and for aerospace and renewable energy applications, and power converter for audio application. He was the CEO of an academic spin-off company and holds three industrial patents. He is the author or co-author of more than 45 papers on top-tier peer-reviewed journals and conferences.

MARCO BINELLI received the B.S. and M.S. degrees in electronic engineering from the University of Parma, Italy, in 2003 and 2006, respectively, and the Ph.D. degree from the University of Parma, in 2010, with a thesis on analysis and equalization techniques in automotive acoustics.

Since 2010, he has been a Research Fellow with the University of Parma. His research interests include equalization, microphones and loudspeakers arrays, spatial audio psychoacoustics, and active noise control.

ANGELO FARINA received the M.S. degree in civil engineering from the University of Bologna, Italy, in December 1982, and the Ph.D. degree in technical physics from the University of Bologna, in 1987.

In May 2005, he became a Full Professor in environmental applied physics with the University of Parma. He is the author of more than 300 scientific articles. His research interests include applied acoustics, including noise and vibration, concert hall acoustics, simulation software, advanced measurement systems, microphone, and loudspeaker arrays. He was awarded with the Audio Engineering Society Fellowship for his pioneering work on electroacoustic measurements based on exponential sine sweeps.

STEFANO MAGLIA received the M.S. degree in mechanical engineering from the University of Brescia, Italy, in 2002, with specialization in structural engineering. Enrolled in the Order of Engineers of Cremona, since 2005, he conducts his professional activity in industrial companies, in the milling, energy, cogeneration from syngas, biogas and natural gas, production of biomethane and derivatives, and dealing with the design of machines and systems, since 2008, for AB Impianti Srl Company.

JESSICA FERRARI received the B.S. and M.S. degrees in management engineering from the University of Parma, Italy, in March 2018. She is currently pursuing the Ph.D. degree in industrial engineering. Her B.S. thesis "Dealing in commodity market: analysis and correction of ambient reverberation." She is also achieving the license to practice as an Engineer.

ANDREA ZENARO received the M.S. degree in chemistry from the University of Padova and the master's degree in electroacoustics from the University of Modena and Reggio Emilia, in 2018. Enrolled in the Order of Chemistry, in 2020, he conducts his professional activity in environmental acoustics for AB Impianti Srl Company, since 2021.

ENRICO CALZAVACCA received the M.S. degree in electronic engineering from the University of Brescia, Italy, in 1998. He has been an Engineer with the Renewable Energy Sector, since 2003. He has been the Technical Director, since 2007, and the Research and Development Director of AB Impianti Srl, since 2017. His research interests include energy efficiency and ecological transition, especially focusing on equipment for renewable gases and carbon dioxide capture and use. Since 2022, he has been a member of the Teaching Board of the Energy Transition Ph.D. with the University of Brescia.

· · ·